Impact of the Detected Scintillation Light Intensity on Neutron-Gamma Discrimination

Massimo Caccia, Marco Galoppo, Luca Malinverno, Pietro Monti-Guarnieri, and Romualdo Santoro

***Abstract*— This article reports the method and the results of a study on the impact of the detected light intensity on gamma-neutron discrimination. In particular, the minimum number of photons required to achieve a statistically significant separation was measured and shown to be stable against a variation of the photon detection efficiency (PDE) of the system under study. The method, developed using an EJ-276 scintillator bar coupled to a silicon photomultiplier (SiPM), is of general interest. For this specific system, the minimum statistic was measured to be 317 ± 16 photons, corresponding to different values of the deposited energy, as the PDE was changed.**

***Index Terms*— Neutron-gamma discrimination, photon statistics, plastic scintillators, pulse shape analysis, silicon photomultipliers (SiPM).**

I. Introduction

SILICON photomultipliers (SiPMs hereafter) are compact solid-state light detectors with single photon sensitivity, photon counting capability, low bias voltage, and low power consumption. In the last decade, SiPMs have been used in a variety of fields, such as particle and nuclear physics, medical imaging, and homeland security [1], [2], [3]. It has been shown that SiPMs, coupled to specifically engineered scintillators with sensitivity to both fast and slow neutrons, represent a viable solution for the discrimination of light pulses originated by gamma rays against neutrons [4]. The enabling feature of this class of scintillators is the different light emission time in response to interactions of neutrons or gamma rays. Hence, a pulse shape analysis is usually implemented by defining a pulse shape discrimination (PSD) observable [5], [6], [7], [8], [9], [10], [11].

For every detection system used for particle identification there exists a critical condition for which the signal produced by the impinging radiation does not convey enough information to achieve particle discrimination. This effect usually manifests itself through the existence of a system-specific energy deposit threshold below which the identification capability is lost. In the case of a scintillator coupled to a light sensor, the energy deposit and thus the information carried by the signal is directly related to the intensity of the scintillation light. The idea behind this study is to investigate the correlation between the minimum amount of information required for particle discrimination and the photon statistics.

The results of the investigation reported here stems from a system based on a plastic scintillator (EJ-276, by Eljen Technologies) coupled to a SiPM, where the response and sensitivity were changed by varying the photon detection efficiency (PDE) of the SiPM, acting on the biasing voltage. The outcome of this study is the definition of a procedure having a general applicability that not only sheds light on the correlation between the photon statistics and the information conveyed by the signal but also yields the minimum photon statistics required for neutron-gamma discrimination.

TABLE I

MAIN FIGURES OF THE SENSORS IN USE, AS OF THE VENDOR'S SPECIFICATIONS

Hamamatsu S13360-6050PE	
Pixel pitch	$50\,\mu m$
V_{bd}^{a}	$53 \pm 5\,V$
V_{op}^{b}	$V_{bd} + 3\,V$
Terminal capacitance C_t	$1280\,pF$
Dark count rate	$2000\,kHz$
Crosstalk probability	3%
PDE[c]	40%

[a] V_{bd} identifies the breakdown voltage. The uncertainty refers to lot-to-lot variations.
[b] V_{op} is the suggested operational voltage
[c] The PDE corresponds to the peak value ($\lambda = 450\,nm$), at V_{op} and $T = 25°\,C$.

II. Materials and Methods

The analysis is based on a 6 mm × 6 mm area SiPM produced by HAMAMATSU Photonics (model S13360-6050PE), with the main features reported in Table I, as of the vendor's specifications [12].

The sensor was coupled through optical grease to a 5 cm × 1 cm × 1 cm EJ-276 scintillator bar produced by Eljen Technologies, where pulse shape neutron-gamma discrimination is made possible by the differences in the scintillating time decay constants, as reported in Table II [13]. The bar was wrapped with Teflon tape diffuser to maximize light collection and the assembly was operated in a light-tight box to prevent contamination from ambient light.

The energy calibration was performed exploiting the Compton spectrum shoulder for a series of gamma emitting isotopes

Manuscript received 2 February 2022; revised 6 June 2022 and 5 July 2022; accepted 22 August 2022. Date of publication 5 September 2022; date of current version 18 October 2022.

The authors are with the Dipartimento di Scienza e Alta Tecnologia, Universitá degli Studi dell'Insubria, 22100 Como, Italy (e-mail: massimo.caccia@uninsubria.it).

Color versions of one or more figures in this article are available at https://doi.org/10.1109/TNS.2022.3203819.

Digital Object Identifier 10.1109/TNS.2022.3203819

TABLE II
MAIN FIGURES OF THE EJ-276 FAST NEUTRON SENSITIVE SCINTILLATOR

Eljen EJ276	
τ_1 $(\gamma\&n)$	13 ns
τ_2 (γ/n)	30/50 ns
τ_3 (γ/n)	270/460 ns
Photons/MeV	8600
Density	1.0096 $[g/cm^3]$
λ_{peak}	425 nm

TABLE III
ENERGIES OF THE COMPTON EDGES

Source	E_γ [keV]	Branching Ratio	E_{edge} [keV]
^{22}Na	511		341
	1275		1062
^{60}Co	1173	99.85%	1040 (mean) [a]
	1332	99.98%	
^{133}Ba	276	7.13%	196 (mean)
	303	18.31%	
	356	62.05%	
	384	8.94%	
^{137}Cs	662		478

[a] E_{edge} is the mean value, weighted by the branching ratios.

(^{22}Na, ^{60}Co, ^{133}Ba, and ^{137}Cs). Neutron–gamma discrimination was instead investigated using a ^{252}Cf source.

The system response in terms of detected photons per pulse was measured after a calibration performed by illuminating the sensor with an ultrafast blue LED emitting at 420 nm, pulsed by a PicoQuant PDL-800B unit.

For γ and neutron detection, the signal produced by the SiPM was directly digitized with a CAEN DT5720 Desktop Digitizer (sampling frequency 250 mega-samples/s, 12-bit resolution, 2-V input range). For the calibration in photoelectrons, the signals were amplified using the CAEN SP5600 unit, featuring a variable gain in the 0-50-dB range.

A. Energy Calibration

Due to the low Z and density of the plastic scintillator, the gamma rays rarely interact through photoelectric effect. Hence, calibrations relied on the Compton spectrum shoulders. The energy associated with the edge of a shoulder, E_{edge}, can be derived from the theory of the Compton scattering [14] and is given by

$$E_{\text{edge}} = \frac{E_\gamma^2}{2E_\gamma + m_e c^2} \tag{1}$$

where $m_e c^2$ is the energy of the electron at rest and E_γ is the γ ray energy or the weighted mean of multiple lines not resolved in the experimental spectrum (with the weights being the emission branching ratios). The edge shoulders used in the calibration are reported in Table III.

For these measurements, the DT5720 unit was self-triggered and signals exceeding a fixed threshold were sampled and digitized over a 8 μs long window, with the signal peak located 2 μs after the digitization gate opening. For every run at different conditions, about 250 000 pulses were recorded. For the duration of all experiments and the measurements of the main sensor figures, the SiPM was maintained at constant temperature of 18.0 °C ± 0.1 °C.

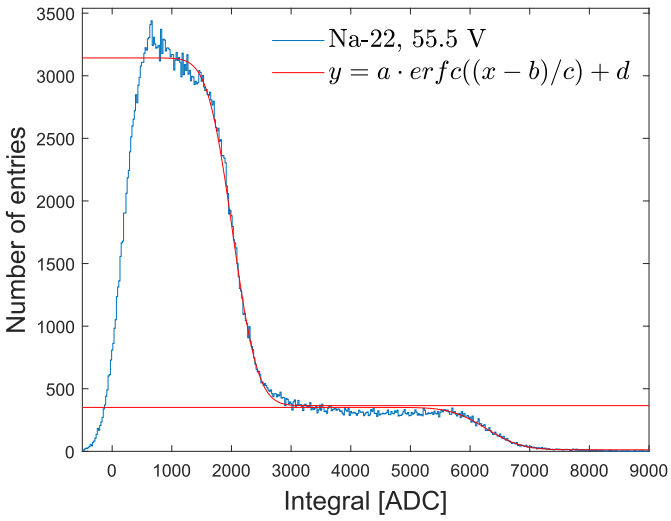

Fig. 1. Energy spectrum of the ^{22}Na source, obtained at 55.5 V (4 V above the breakdown voltage) and shown altogether with the error function fit on the Compton edge.

The calibration was repeated for every SiPM biasing voltage used to evaluate the impact of a PDE variation, namely from 3 to 6.5 V above the breakdown voltage, at 0.5 V steps.

During data processing, the signal baseline was calculated for every waveform over 400 ns (100 points) before the trigger and then subtracted. The occasional occurrence of a spurious pulse dark count during the baseline calculation was identified by an anomalous standard deviation of the data points; moreover, piled-up events in the digitization window following the trigger were spotted by identifying a second signal peak. Whenever a waveform featured one of these anomalies, it was flagged and removed from the dataset.

The Compton edges were modeled as step functions, appearing in the spectra as complementary error functions due to their convolution with the response function of the detector which is assumed to be Gaussian. An exemplary spectrum of the ^{22}Na source, obtained by biasing the sensor at 55.5 V (which corresponds to 4 V above the breakdown voltage), is reported in Fig. 1. A typical calibration line at a fixed bias is shown in Fig. 2.

B. Photoelectron Calibration

The charge corresponding to the avalanche generated in the silicon matrix by a single initial photoelectron depends on the gain of the SiPM, which is linked to the excess voltage, and the external amplification stage. It was measured by analyzing for each specific setting the multiphoton spectrum, namely the histogram characterizing the sensor response to a low plurality of photons emitted by the ultrafast blue LED pulsed by the PicoQuant unit. An exemplary spectrum is shown in Fig. 3, where peaks correspond to the number of fired cells for every pulse, determined by the detected photons and the prompt optical crosstalk, while the significant background between the peaks is connected to delayed optical crosstalk, after pulsing and occasional spurious pulses (dark counts) occurring within the integration window. The shape of the histogram results from the convolution of the Poissonian distribution of emitted

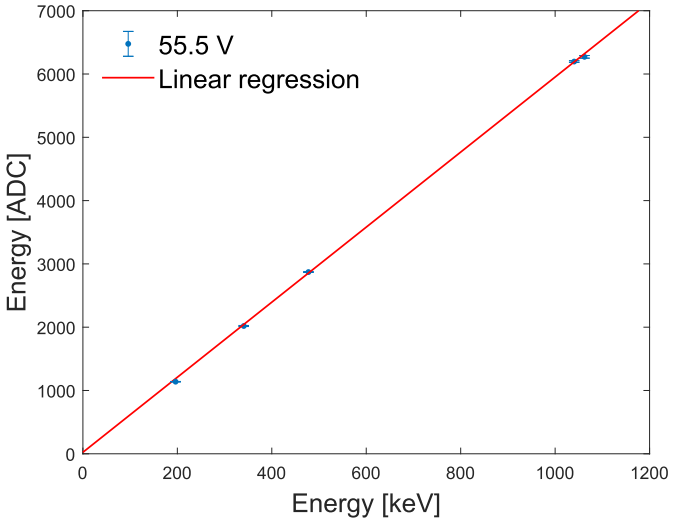

Fig. 2. Calibration line at 55.5 V (4 V above the breakdown voltage), obtained by using the sources reported in Table III.

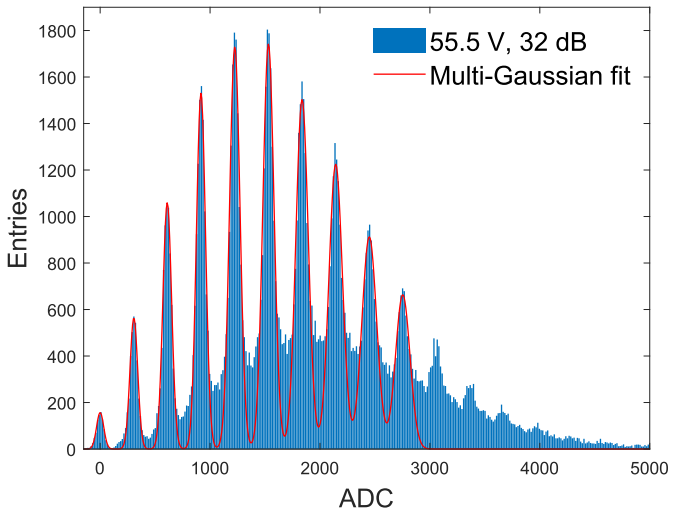

Fig. 3. Frequency histogram of the integrals of the signals (multiphoton spectrum) obtained at 55.5 V (4 V above the breakdown voltage) and amplification gain 32 dB.

photons and the probability distributions of crosstalk and after pulsing. Since the main goal of the procedure is determining the calibration of the sensor response in photoelectrons (number of fired cells), the quantity of interest here is the peak-to-peak distance (Δ_{pp}), providing the single pulse charge in ADC channel at the specified voltage and amplification gain. The single photon signal at gain $G = 1$ (Δ^1_{pp}) and at fixed bias V, namely the condition in use for gamma and neutron detection, was measured by extrapolating the values of Δ_{pp} at different amplification settings, as shown for instance in Fig. 4, again for the reference bias of 55.5 V (4 V above the breakdown voltage). A residual difference between digitization and integration of the direct output of the SiPM, dc coupled to the input of the digitizer, and the gain 1 setting of the ac coupled amplifier in the SP5600 unit was measured comparing the most probable value of the response of the system in the two configurations to a high light intensity pulsed illumination. This procedure lead to a final scaling factor

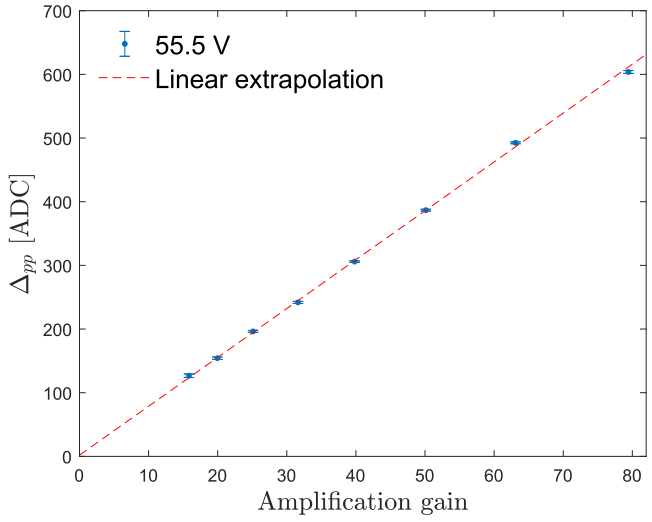

Fig. 4. Variation of the delta peak-to-peak Δ_{pp} as a function of the amplification gain G, for fixed biasing voltage 55.5 V. Linear extrapolation in the form $\Delta_{\mathrm{pp}} = m \cdot G + q$, with $m = 7.67 \pm 0.03$, and $q = 1.96 \pm 1.49$.

$k_{\mathrm{ac/dc}} = 0.8830 \pm 0.0001$, taken into account when calibrating the energy response in photoelectrons.

Moreover, the multiphoton spectrum offers the possibility to measure the following.

- The optical crosstalk, fitting the spectrum with the convolution of the Poisson probability describing photon emission by a pulsed light source and the geometrical distribution for the crosstalk [15]. This figure is required to extract the statistics of primary photoelectrons in pulses originated by gamma and neutrons.
- The relative PDE by a variation of the mean number of detected photons in a pulse at constant illumination for different SiPM biasing voltages [16].

As by-product of this analysis, the breakdown voltage of the sensor was also calculated as the value of V where Δ_{pp} is null.

For these measurements, the data acquisition was synchronous to the PicoQuant pulsing, and signals were digitized over a 4 μs long window, with the peak of the signal located 2 μs after its opening. For every run at different conditions, about 150 000 pulses were digitized, recorded, integrated, and histogrammed. A multi-Gaussian function was fit over every spectrum, in order to calculate Δ_{pp}, defined as the mean distance between adjacent peaks. This procedure was repeated for amplification gains ranging from 24 to 38 dB with step 2 dB and biasing voltages ranging from 54.5 V (3 V above the breakdown voltage) to 58 V (6.5 V above the breakdown voltage). By the end of this analysis, an extrapolation of Δ_{pp} values obtained at different voltages and gain 32 dB returned a breakdown voltage $V_{\mathrm{bd}} = 51.42 \pm 0.04$ V.

The optical crosstalk and the variation of the PDE with the biasing voltage were extracted by the same dataset. However, it was instrumental to process the data to produce multiphoton spectra based on the use of the peak value of every waveform rather than the integral, since detector-related spurious effects, notably after pulses, delayed crosstalk and dark counts are expected not to come into play. This is evident in the

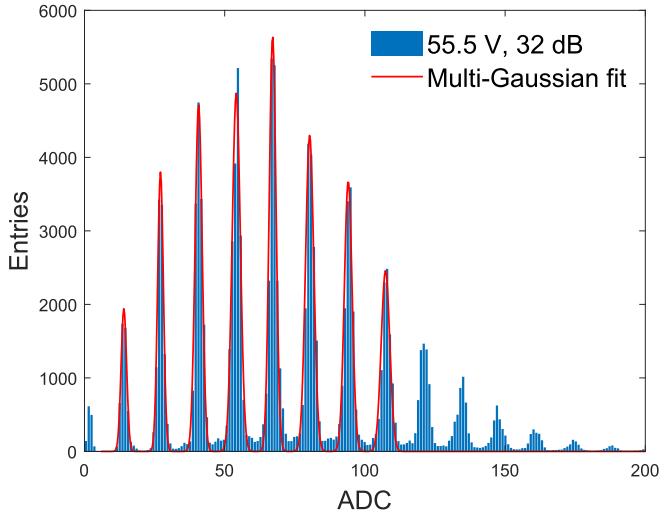

Fig. 5. Frequency histogram of the amplitudes of the signals (pulse-height multiphoton spectrum) obtained at 55.5 V (4 V above the breakdown voltage) and amplification gain 32 dB.

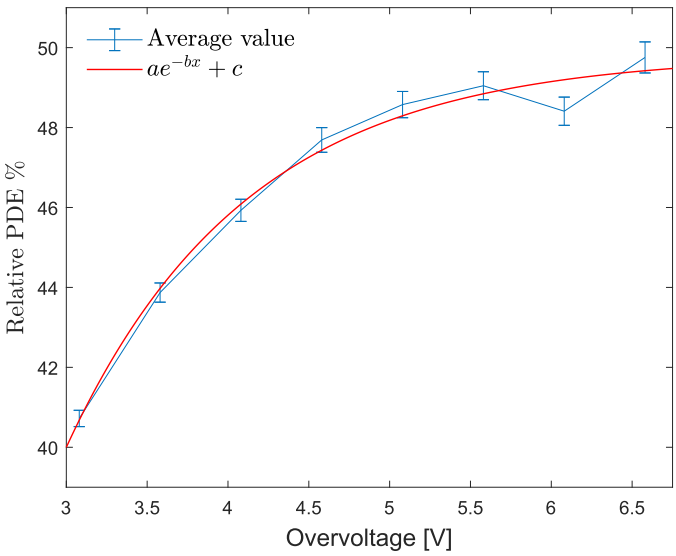

Fig. 6. Relative PDE of the sensor as a function of the bias voltage. The values shown are the average of the PDE evaluated at every gain available.

exemplary spectrum shown in Fig. 5, again for the reference bias 55.5 V.

Once Δ_{pp} is known, the average value of the amplitude distribution can be converted into number of fired cells (μ_{exp}). This value accounts for the number of detected photons μ_0 and the effective optical crosstalk X, with a dependence that can be modeled as [17]

$$\mu_{\text{exp}} = \frac{\mu_0}{1 - X}. \tag{2}$$

Under the assumption of a Poissonian distribution of emitted photons, the value of μ_0 can be obtained as

$$\mu_0 = -\log(P_0) \tag{3}$$

where P_0, the probability of having 0 fired cells, can be simply calculated as the fraction of the events with a pulse height $\leq 0.5 \times \Delta_{\text{pp}}$. Experimentally, crosstalk probabilities ranging from 13% to 25% were measured, corresponding to biasing voltages ranging from 3 to 6.5 V above the breakdown voltage.

Since μ_0 is proportional to the PDE of the sensor, its trend against biasing voltage variations actually maps changes in the PDE. Results are shown in Fig. 6, normalized according to the producer's specifications, namely PDE $= 40\%$ at $V_{\text{ov}} = 3$ V.

C. Neutron-Gamma Discrimination

As of the characterization reported in [3] and the comparative analysis performed in [18], neutron-gamma discrimination was based on a PSD variable corresponding to the energy deposited in the tail of the signal, normalized to the pulse height

$$\text{PSD} = \frac{\int_{t_s}^{t_s+t_w} S(t)dt}{\max\{S(t)\}} \tag{4}$$

where $S(t)$ is the digitized signal, t_s marks the beginning of the tail, and t_w its length. The optimal limits for the tail integration were identified by scanning the parameter space and identifying the region with the highest discrimination power, quantified by a figure of merit (FOM) defined as [14]

$$\text{FOM} = \frac{\overline{\text{PSD}}_n - \overline{\text{PSD}}_\gamma}{\text{FWHM}_n + \text{FWHM}\gamma} \tag{5}$$

where $\overline{\text{PSD}}_n$ and $\overline{\text{PSD}}_\gamma$ correspond to the mean values of the PSD distributions for gamma rays and neutrons, respectively, while FWHM_n and FWHM_γ are their full-width at half-maximum. Discrimination is assumed to be statistically relevant when FOM > 1.27, corresponding to a 3σ separation between the distributions of the PSD variables for neutrons and gammas, presumed to be Gaussians.

For each biasing voltage, on average, 500 000 events were recorded, digitized, and analyzed. Fig. 7 shows an exemplary outcome of the optimization procedure of the algorithm, showing the variation of the FOM against the PSDs parameters

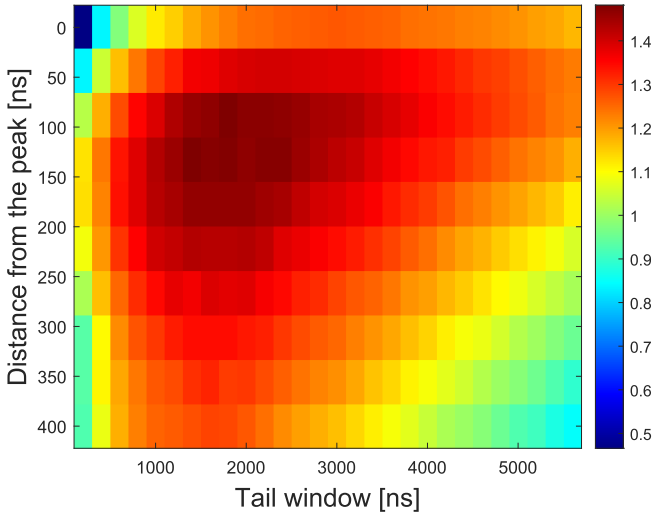

Fig. 7. Variation of the FOM, as a function of the PSD parameters t_s ("distance from the peak") and t_w ("tail window"), as used in (4). The FOM was calculated, for every set of parameters, by means of (5).

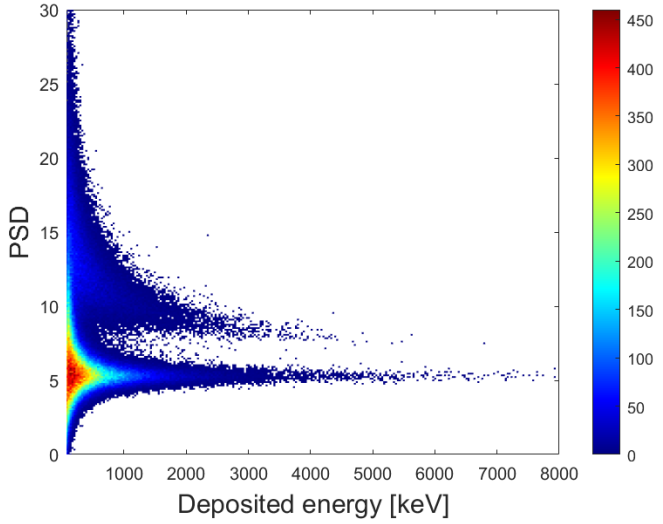

Fig. 8. Two-dimensional histogram of the PSD values against the deposited energies recorded with the ^{252}Cf source, biasing the SiPM at 55.5 V (4 V above the breakdown voltage). The deposited energies results by the calibration coefficients as of Section II-A. The upper branch of the plot represents neutron detection.

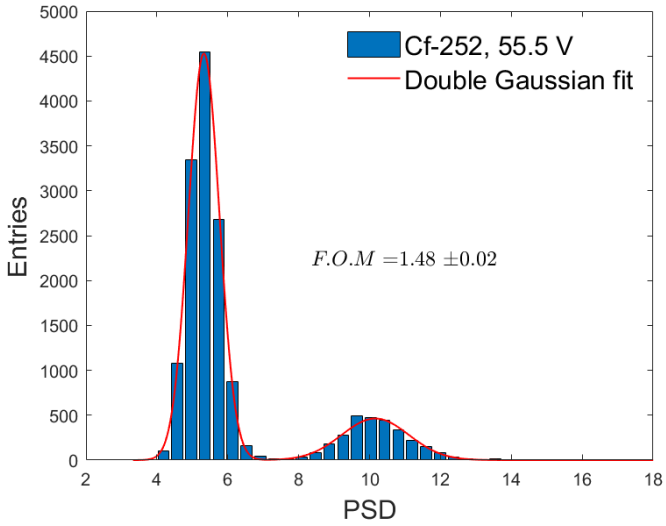

Fig. 9. Histogram of the PSDs shown in Fig. 8, obtained by biasing the SiPM at 55.5 V (4 V above the breakdown voltage) and considering only the events with energy E inside the projection window 1 MeV $\leq E \leq$ 1.5 MeV. The geometric separation between the fit curves gives the FOM, as indicated in (5).

t_s, t_w (data recorded at the reference bias of 55.5 V). Fig. 8 shows an exemplary 2-D histogram of the PSD values against the deposited energy in response to ^{252}Cf: here gammas and neutrons form two clearly separated regions, for energies above 1 MeV. An exemplary distribution of the PSD values in the [1, 1.5] MeV range of deposited energy is shown in Fig. 9.

III. Experimental Results

For every excess voltage, namely for every PDE, the value of the deposited energy required to achieve FOM = 1.27 was estimated by analyzing the PSD variable distribution in different deposited energy bins, initially 100 keV wide for edges ranging from 150 keV to 1 MeV. Subsequently, the width was doubled at every bin, in order to compensate for the smaller

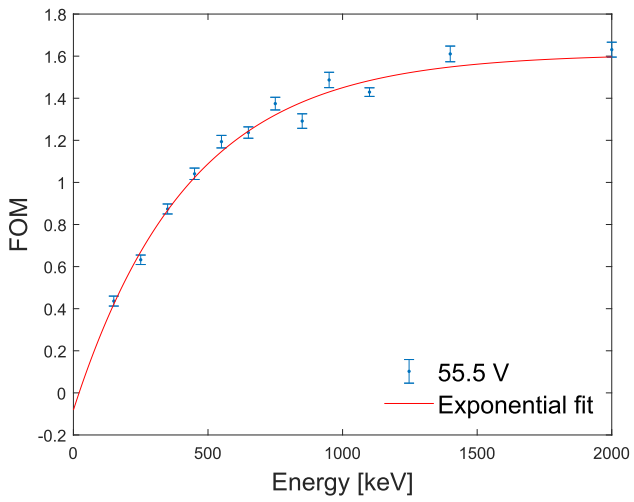

Fig. 10. Variation of the FOM as a result of the different choice in the energy projection windows. The values represented on the x-axis correspond to the center of the energy bins.

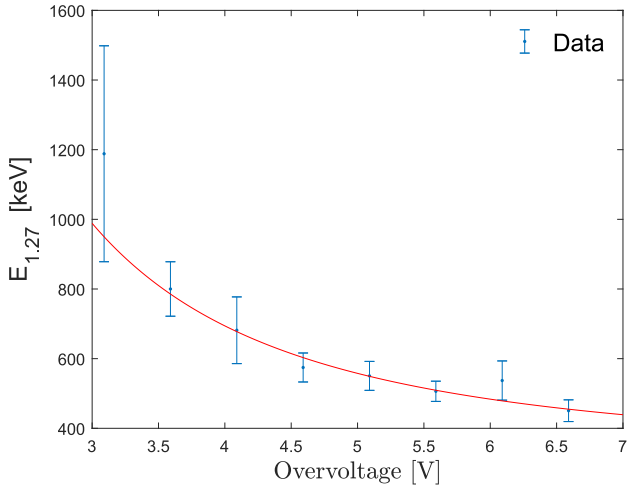

Fig. 11. Minimum energy necessary to reach FOM = 1.27 as a function of the over-voltage applied to sensor. The line is simply meant to guide the eye.

size of the sample as the energy increased. The minimum energy necessary to reach FOM = 1.27 ($E_{1.27}$) was calculated by fitting the variation of the FOM with respect to the energy by means of an exponential function

$$\mathrm{FOM}(E) = a \cdot \left(1 - e^{-[(E-b)/c]}\right). \tag{6}$$

An exemplary trend of the FOM variation at the 55.5 V reference voltage is shown in Fig. 10.

The minimum number of photoelectrons corresponding to an energy deposit of $E_{1.27}$, namely $N_{1.27}$, can be derived through the calibration of the deposited energy in photoelectrons taking into account the effective crosstalk and $k_{\mathrm{ac/dc}}$, namely

$$N_{1.27} = (m \cdot E_{1.27} + q)\frac{k_{\mathrm{ac/dc}}}{\Delta^1_{\mathrm{pp}}}(1 - X) \tag{7}$$

whereas Δ^1_{pp} is the Δ_{pp} extrapolated at linear gain $G = 1$ and m, q are the energy calibration coefficients.

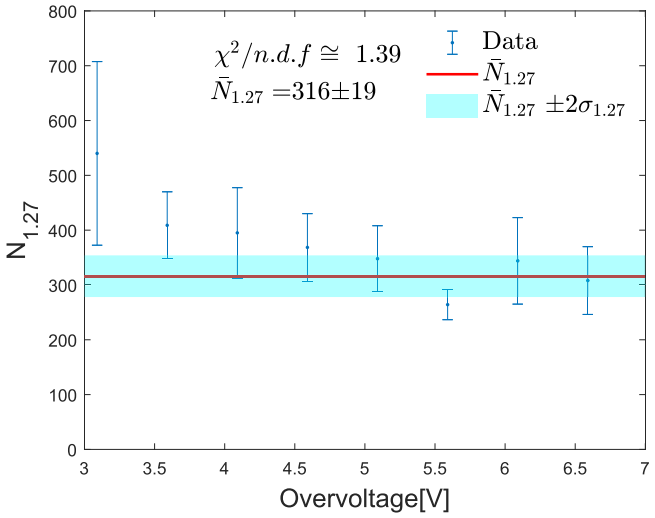

Fig. 12. Minimum number of photoelectrons ($N_{1.27}$) required to reach FOM = 1.27. The dotted red line shows the weighted mean of the data and the cyan area corresponds to an interval of two standard deviations ($\pm\sigma_{1.27}$) with respect to the mean. The χ^2 value shows a fair agreement with the hypothesis of having a constant $N_{1.27}$ as the operational conditions are changed.

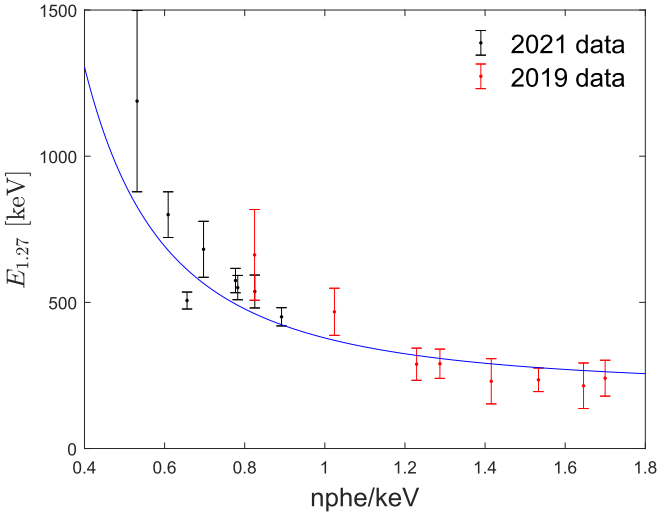

Fig. 13. Minimum energy deposit corresponding to FOM = 1.27 (i.e., $E_{1.27}$) shown as a function of the number of photoelectrons extracted per keV of energy deposit. The label "2021 data" refers to the first dataset analyzed in the article, i.e., the one with an EJ-276 bar without aging effects. The label "2019 data" refers to the higher light yield dataset. The line is simply meant to guide the eye.

The variation of $E_{1.27}$ as a function of the over-voltage of the sensor (V_{ov}) is shown in Fig. 11, with a statistically significant decreasing trend as expected by the PDE variation. However, when $E_{1.27}$ values are turned into photoelectrons, experimental data correspond to the results shown in Fig. 12, where the hypothesis of a constant "minimum amount of information," corresponding to 316 ± 19 photoelectrons is statistically acceptable.

In order to verify this conclusion, data presented so far were complemented by a different set, coupling a bar of the same EJ-276 scintillator with a higher light yield to a SiPM from the same family. Difference in the light yield was possibly due to aging in the scintillation properties, with the two bars tested right after the delivery by the producer and

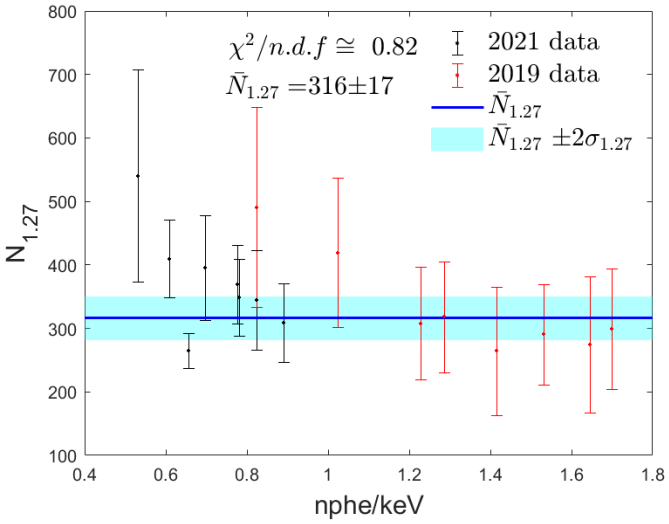

Fig. 14. Minimum number of detected photons ($N_{1.27}$) required to reach FOM = 1.27 shown as a function of the system sensitivity (in terms of p.e./keV). The labels "2021 data" "2019 data" are used in the same sense of Fig. 13. The blue line corresponds to the weighted mean and the χ^2 value shows a fair agreement with the hypothesis of having a constant $N_{1.27}$ as the operational conditions are changed.

after three years on the shelf. Since the two detectors were tested at different over-voltages and featured differences in the PDE, data were displayed against number of photoelectrons per keV of deposited energy. Data on the trend of $E_{1.27}$ are shown in Fig. 13, where the dependence on the system sensitivity is made stronger, while the corresponding number $N_{1.27}$ of photoelectrons is shown in Fig. 14. The weighted mean number of photoelectrons required to reach FOM = 1.27 was found to be, in the two datasets

$$\begin{cases} N^a_{1.27} = 316 \pm 19 \\ N^b_{1.27} = 314 \pm 35. \end{cases}$$

The statistical compatibility of the results confirms the hypothesis of linking the minimum value of deposited energy for discriminating gamma from neutrons to the photoelectron statistics, with a combined value for the specific system under study of $N_{1.27} = 316 \pm 17$.

IV. Conclusion

A neutron-sensitive plastic scintillator bar (EJ-276 by Eljen Technologies) coupled to an SiPM has been used to investigate the impact of the detected light intensity on neutron-gamma discrimination based on pulse shape analysis. The single photon sensitivity of SiPM has been exploited to go from a qualification based on a macroscopic observable, the minimum deposited energy for a statistically relevant discrimination, to the corresponding microscopic quantity, namely the number of detected scintillation photons. For the system under study and the implemented algorithm, based on the ratio between the signal peak value and the integral in the tail of the pulse over an optimal window, 316 ± 17 photoelectrons are required to discriminate pulses originated from gamma rays and neutrons. The value was shown to correspond to different deposited energy values as the PDE was changed in a controlled way for the sake of the investigation.

Apart from quantifying the rather obvious need for a high light yield material and optimal coupling to a highly sensitive photon detector, the method sheds light on the possibility to compare different gamma-neutron discrimination algorithms and procedures, qualified according to the efficiency in extracting information from the available statistics of photons and robustness against statistical fluctuations.

REFERENCES

[1] R. Klanner and F. Sauli, "Silicon photomultipliers: Technology, characterisation and applications," *Nucl. Instrum. Methods Phys. Res. A, Accel. Spectrom. Detect. Assoc. Equip.*, vol. 926, pp. 1–152, May 2019.

[2] S. West *et al.*, "Compact readout of large CLYC scintillators with silicon photomultipler arrays," *Nucl. Instrum. Methods Phys. Res. A, Accel. Spectrom. Detect. Assoc. Equip.*, vol. 951, Jan. 2020, Art. no. 162928.

[3] R. Santoro *et al.*, "Qualification of a compact neutron detector based on SiPM," *J. Instrum.*, vol. 15, no. 5, May 2020, Art. no. C05053.

[4] R. M. Preston, J. E. Eberhardt, and J. R. Tickner, "Neutron-gamma pulse shape discrimination using organic scintillators with silicon photomultiplier readout," *IEEE Trans. Nucl. Sci.*, vol. 61, no. 4, pp. 2410–2418, Aug. 2014.

[5] N. Dinar, D. Celeste, M. Silari, V. Varoli, and A. Fazzi, "Pulse shape discrimination of CLYC scintillator coupled with a large SiPM array," *Nucl. Instrum. Methods Phys. Res. A, Accel. Spectrom. Detect. Assoc. Equip.*, vol. 935, pp. 35–39, Aug. 2019.

[6] C. Liao and H. Yang, "Pulse shape discrimination using EJ-299–33 plastic scintillator coupled with a silicon photomultiplier array," *Nucl. Instrum. Methods Phys. Res. A, Accel. Spectrom. Detect. Assoc. Equip.*, vol. 789, pp. 150–157, Jul. 2015.

[7] M. L. Ruch, M. Flaska, and S. A. Pozzi, "Pulse shape discrimination performance of stilbene coupled to low-noise silicon photomultipliers," *Nucl. Instrum. Methods Phys. Res. A, Accel. Spectrom. Detect. Assoc. Equip.*, vol. 793, pp. 1–5, Sep. 2015.

[8] M. P. Taggart *et al.*, "Fast-neutron response of the novel scintillator caesium hafnium chloride," *Nucl. Instrum. Methods Phys. Res. A, Accel. Spectrom. Detect. Assoc. Equip.*, vol. 1012, Oct. 2021, Art. no. 165224.

[9] M. Grodzicka-Kobylka *et al.*, "Fast neutron and gamma ray pulse shape discrimination in EJ-276 and EJ-276G plastic scintillators," *J. Instrum.*, vol. 15, no. 3, Mar. 2020, Art. no. P03030.

[10] T. Huang and Z. Zhang, "Characterization of 1-inch CLYC scintillator coupled with 8×8 SiPM array," *Nucl. Instrum. Methods Phys. Res. A, Accel. Spectrom. Detect. Assoc. Equip.*, vol. 999, May 2021, Art. no. 165225.

[11] M. P. Taggart, M. Nakhostin, and P. J. Sellin, "Investigation into the potential of GAGG:Ce as a neutron detector," *Nucl. Instrum. Methods Phys. Res. A, Accel. Spectrom. Detect. Assoc. Equip.*, vol. 931, pp. 121–126, Jul. 2019.

[12] HAMAMATSU Photonics. (2010). *Multi-Pixel Photon Counter (MPPC)—S13360 Series*. [Online]. Available: https://www.hamamatsu.com/resources/pdf/ssd/s13360_serie_kapd1052e.pdf

[13] Eljen Technologies. (2011). *Pulse Shape Discrimination EJ-276 & EJ-276G*. [Online]. Available: https://eljentechnology.com/products/plastic-scintillators/ej-276

[14] M. P. Taggart and P. J. Sellin, "Comparison of the pulse shape discrimination performance of plastic scintillators coupled to a SiPM," *Nucl. Instrum. Methods Phys. Res. A, Accel. Spectrom. Detect. Assoc. Equip.*, vol. 908, pp. 148–154, Nov. 2018.

[15] V. Arosio *et al.*, "Reconstruction of the statistics of photons by a pulsed LED using a silicon photomultiplier based set-up," *J. Instrum.*, vol. 10, no. 8, Aug. 2015, Art. no. C08008.

[16] M. Antonello *et al.*, "Tests of a dual-readout fiber calorimeter with SiPM light sensors," *Nucl. Instrum. Methods Phys. Res. A, Accel. Spectrom. Detect. Assoc. Equip.*, vol. 899, pp. 52–64, Aug. 2018.

[17] C. Piemonte and A. Gola, "Overview on the main parameters and technology of modern silicon photomultipliers," *Nucl. Instrum. Methods Phys. Res. A, Accel. Spectrom. Detect. Assoc. Equip.*, vol. 926, pp. 2–15, May 2019.

[18] L. Malinverno, "An optimisation procedure for pulse shape discrimination algorithms tailored for hand-held nuclear security instruments," *Il Nuovo Cimento*, vol. 41, no. 3, p. 123, 2018.

Open Access funding provided by 'Università degli Studi dell'Insubria' within the CRUI CARE Agreement